Measurement of the Electronic Properties of the Flavoprotein Old Yellow Enzyme (OYE) and the OYE:*p*-Cl Phenol Charge-Transfer Complex Using Stark Spectroscopy†

Nancy Hopkins‡ and Robert J. Stanley*,§

Department of Chemistry, Rutgers University, 315 Penn Street, Camden, New Jersey 08102, and Department of Chemistry, Temple University, 201 Beury Hall, Philadelphia, Pennsylvania 19122

Received September 23, 2002; Revised Manuscript Received November 19, 2002

ABSTRACT: Low-temperature absorption and Stark spectroscopy have been used to study the electronic properties of oxidized flavin mononucleotide (FMN) in old yellow enzyme (OYE) and OYE complexed with *p*-chlorophenol (*p*-Cl phenol). The low-temperature absorbance spectrum of OYE showed splittings of the blue and near-UV vibronic bands, which appears to be due to hydrogen bonding between the isoalloxazine moiety and the protein. A Stark spectroscopic analysis showed that the electronic structure of the FMN cofactor in OYE is not significantly perturbed relative to flavins in simple solvents. However, the charge-transfer band in the OYE:*p*-Cl phenol complex showed a large Stark effect indicative of substantial charge displacement. The magnitude and direction of this charge displacement are consistent with significant charge transfer along the charge-transfer transition dipole moment direction. In addition, the Stark spectrum of the CT band showed unexpected fine structure that could correlate with vibrational progressions in either the *p*-Cl phenol donor or the flavin acceptor.

A unique property of flavins is the ability to form charge-transfer complexes with a variety of donors and acceptors (*1*). These charge-transfer (CT)[1] complexes are often discovered by the observation of a new spectral band that is red-shifted from the intrinsic absorption spectrum of the isoalloxazine ring (*2*). The interest in these charge-transfer bands is multifaceted. Charge-transfer complexes have been shown to affect the midpoint potentials of flavoproteins, and this may be important in poising the midpoint potential of the flavin relative to other molecules during a redox process (*3*). In addition, they may be important in stabilizing small ligand molecules in the protein to enhance the overall rate of catalysis (*2*). Many flavoproteins exhibit charge-transfer intermediates during their catalytic cycle, such as the FAD_{ox}−(S^-Cysteine-) and NAD^+−$FADH^-$ charge-transfer complexes observed in lipoamide dehydrogenase during the reductive half of the reaction (*4*, *5*). These complexes can form with exogenous donors/acceptors or with amino acid groups such as tryptophan (*6*).

With relatively few exceptions (*2*, *3*, *7*), there is not much evidence addressing the significance of the CT band in the functioning of a flavoprotein. We think this is because CT bands appear when CT itself is functionally irrelevant. This will be the case when CT is manifested primarily in the excited electronic state of the complex rather than the ground state where redox chemistry occurs. Of course, excited-state charge transfer can be critical in the case of light-driven flavoproteins such as DNA photolyase (*8*) where photoinduced electron transfer is central to function. However, the mere appearance of a CT band does not guarantee that significant charge transfer occurs in the ground state where it can have functional consequences. Indeed, while many theoretical approaches start out by assuming that the ground state of a complex will have some CT character (*9*), the usual procedure is to assume that the amount of CT is negligible as compared to the excited state (*10*). This approximation is probably not valid when the ionization potential of the donor is relatively low, as in the case of the negative ions of amino acids such as Cysteine but may be perfectly reasonable when tryptophan acts as a donor to an excited flavin molecule as has been observed in protein and model systems (*6*, *11*). Thus, the effect of CT complexation on the redox potential and function of flavoenzymes is still open to discovery. A more molecular level approach would be invaluable in understanding the detailed interactions between the donor and the acceptor in a protein.

As a first effort in this direction, we will present a Stark spectroscopic analysis of old yellow enzyme (OYE) and its charge-transfer complex with *p*-Cl phenol. It is fitting that the first Stark study of a flavoprotein and its charge-transfer complex begins with the first flavoprotein ever discovered

† N.H. gratefully acknowledges financial support from the Ford Foundation Postdoctoral Fellowship for Minorities. R.J.S. gratefully acknowledges the Petroleum Research Foundation (Grant 35353-G4) and the National Science Foundation (MCB-9982532) for financial support.

* Corresponding author. Phone: (215) 204-2027. Fax: (215) 204-1532. E-mail: robert.stanley@temple.edu.

‡ Rutgers University.

§ Temple University.

[1] Abbreviations: FMN, flavin mononucleotide; OYE, old yellow enzyme; *p*-Cl: *para*-chlorophenol; CT, charge transfer; FAD_{ox}, oxidized flavin adenine dinucleotide; NAD^+, nicotinamide adenine dinculeotide phosphate cation; $FADH^-$, fully reduced flavin adenine dinucleotide anion.

10.1021/bi0268908 CCC: $25.00
Published on Web 01/04/2003

Scheme 1

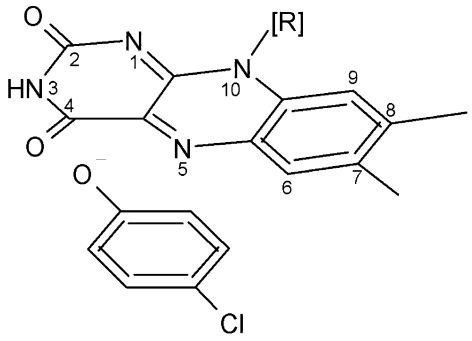

(*12*). OYE is a FMN-containing dimeric enzyme, and its specific function remains a continual scientific pursuit. OYE forms charge-transfer complexes in the presence of phenolate ligands (*3*). For OYE, addition of *p*-Cl phenol to the protein results in an intense broad red-shifted band with concomitant diminution of the flavin $\pi \rightarrow \pi^*$ absorption bands. This new band has been ascribed to a charge-transfer transition where the deprotonated phenolate is the donor, and the flavin is the acceptor (*13*). Scheme 1 shows the approximate orientation (and numbering system) for the FMN:*p*-Cl phenol complex based on the structure of the OYE:*p*-hydroxybenzaldehyde complex (*14*). Massey and Abramovitz observed a correlation between the position of the CT band maximum, $h\nu_{CT}$, and the midpoint potential of the oxidized $\rightarrow$ semiquinone couple for a variety of phenolate ligands (*13*). In addition, these researchers have shown a linear correlation between $h\nu_{CT}$ and the redox potential of modified flavins substituted into apo-OYE, which have different electron affinities (*3*).

Stark spectroscopy (electroabsorption) promises to contribute much to our understanding of charge transfer in flavoproteins (*15*). It has already been used to describe charge-transfer states in photosynthesis (*16*) and in the Cu-containing protein azurin (*17*) but has never been used to study flavoproteins. Stark spectroscopy employs an externally applied electric field to perturb the ground and excited-state energies of the chromophore (*18*). These perturbations arise through the interaction of the applied field with the permanent ground- and excited-state dipole moments ($\vec{\mu}_g$ and $\vec{\mu}_e$) and polarizabilities ($\vec{\vec{\alpha}}_g$ and $\vec{\vec{\alpha}}_e$) of these states. Stark spectra are characterized by spectral shifts and line broadenings that can be analyzed to return the difference dipole moment, $\Delta\vec{\mu} = \vec{\mu}_e - \vec{\mu}_g$, and difference polarizability, $\Delta\vec{\vec{\alpha}} = \vec{\vec{\alpha}}_e - \vec{\vec{\alpha}}_g$ (usually given as $tr\Delta\vec{\vec{\alpha}}$, the average polarizability change) of the states coupled by the absorption of a photon. Stark spectra that appear to be second-derivative with respect to the absorption spectrum indicate a nonzero $\Delta\vec{\mu}$, while first-derivative features indicate that $\Delta\alpha$ is nonzero.

For example (*19*), for flavins in simple solvents Band I ($\sim$450 nm; $S_0 \rightarrow S_1$) is dominated by a change in the dipole moment between S_0 and S_1 of about 1.5 Debye (D). Band II ($\sim$370 nm; $S_0 \rightarrow S_2$) undergoes about a 3-fold increase in $\Delta\vec{\mu}$ (relative to Band I) the change in polarizability, $\Delta\vec{\vec{\alpha}}$, is much larger than that observed for Band I, leading to the conclusion that the S_2 state is much more polarizable than either the S_1 or S_0 states. In addition, the use of polarized light for Stark measurements can return directional information about these electronic structure parameters.

In this contribution we present and analyze the Stark spectra for both OYE and the OYE:*p*-Cl phenol complex. These data show that the long wavelength band observed in the absorption spectrum of the complex is accompanied by a large charge displacement that is out of the plane of the isoalloxazine ring of the FMN cofactor. Our results give compelling evidence that Stark spectroscopy can be used to quantify the degree and direction of charge transfer in flavoproteins. This information will be useful in ascertaining the functional role of charge transfer in the redox chemistry of these proteins.

MATERIALS AND METHODS

OYE Protein and CT Complex. The OYE was a generous gift from Prof. Vincent Massey at the University of Michigan. FMN and *p*-Cl phenol were purchased from Sigma Chemicals. All buffer salts and other reagents were of the highest purity. OYE was dissolved in 0.1 M phosphate (pH 7.0) at a concentration no lower than 200 μM. Room-temperature absorption spectra were obtained using a HP8452A UV−vis photodiode array spectrophotometer. Published extinction coefficients were used in the concentration determinations for OYE and OYE with *p*-Cl phenol (*20*). After the concentration was determined, an equal volume of glycerol was added to give a final value of 50% glycerol. The spectrum was measured, and the concentration was recorded. To obtain the complex, OYE in phosphate buffer and 50% glycerol at approximately 330 μM was incubated with 0.5 mM *p*-Cl phenol. Excess ligand was removed by centrifugation in a 10 000 MWCO concentrator.

Low-Temperature Absorption Spectra. To measure the spectrum at low temperature (77 K), the sample or buffer was loaded into a cuvette of home design. The low-temperature cell was constructed using two 1 in. diameter $\times$ 2 mm thick fused silica windows separated by a 0.05-cm alumina ring with a clear aperture of about 1 cm. This gave a sample with an optical density of about 0.2 at 450 nm at the working concentration. Prior to freezing, the sample was placed in a Speed-Vac for about 5 min to remove dissolved gas and to spin down particulates. If this step was omitted, the frozen glass scattered light to a much greater extent. Scattering was a major difficulty in obtaining accurate low-temperature spectra.

Two methods were used to obtain the low-temperature glass. The cuvette was filled with about 100 μL of protein or buffer. The cuvette was attached to a coldfinger and placed inside a nitrogen purged glass vacuum chamber at ambient pressure. The solution was frozen slowly by adding small amounts of liquid nitrogen to the coldfinger. Once the sample or buffer froze ($\sim$3 min), the chamber was evacuated. Alternatively, the cuvette was plunged into an optical dewar containing liquid nitrogen (H. S. Martin), whereupon the sample froze within a few seconds. The resulting glasses contained optically clear domains of about 2 mm in diameter.

The spectra were recorded in one of two ways for the dewar system. The photodiode array UV−vis spectrometer was used to record the transmission of the buffer and protein solution to give the absorbance. Bubbling and swirling effects inside the dewar required acquisition times of less than 1 s, thereby limiting the signal-to-noise of the spectrum. Absorption spectra were also obtained using the optical bench for

the Stark spectrometer with the addition of a reference photodiode to monitor lamp fluctuations for normalization purposes. Even though this approach uses single wavelength detection, the inclusion of a chopper running at ~3 kHz with lock-in detection reduces somewhat the effects of scattering due to swirling nitrogen and snow build-up in the dewar. This latter detection method was used exclusively with the coldfinger system. The coldfinger approach has the advantage of lower noise but the disadvantage of not being able to obtain the absorption spectrum under identical conditions as the Stark spectrum, which was only obtained in the dewar. Despite this, there is no evidence that absorption spectra obtained using the coldfinger were not equivalent to those obtained in the dewar within the signal-to-noise ratio. The transmission spectrum of the buffer is usually measured first (I_0) and then the sample (I). No correction was made for path length changes at low temperature. The absorbance is calculated from $A = \log(I_0/I)$, and the extinction was calculated from the concentration and path length. Derivatives of the spectra were obtained numerically (Origin 6.0, Microcal).

Stark Spectroscopy. Stark spectra were obtained at low temperature. While low temperature is not a requirement for the technique, it greatly simplifies the interpretation of the spectra. There are two reasons for this. First, if the molecule (i.e., protein) has a significant ground-state dipole moment it can reorient in the applied field. This orientational effect is usually manifested by a change in the extinction coefficient and can be taken care of in the analysis of the spectra, though this complicates the analysis. The use of a frozen glassy matrix such as 1:1 (v/v) glycerol/buffer eliminates this effect. Second, spectral line shapes are narrower at cryogenic temperature. Since the Stark spectrum is essentially a derivative spectrum, the signal is strongly modulated by the line width. A narrow line is much more easily detected than a broad band. This is well-demonstrated by our data.

The analysis of the Stark spectra derives from Liptay (*16*, *18*). The application of an AC electric field during the measurement of the low-temperature absorption spectrum yields a Stark spectrum that can be fitted to derivatives of the zero field absorption spectrum. The field-induced change in the extinction, $\Delta\epsilon$, is related to derivatives of the absorption spectrum, $\epsilon(\nu)$, weighted by the A_χ, B_χ, and C_χ coefficients:

$$\frac{\Delta\epsilon}{\nu} = (f\vec{F})^2\left\{A_\chi\frac{\epsilon(\nu)}{\nu} + \frac{B_\chi}{15hc}\frac{\mathrm{d}[\epsilon(\nu)/\nu]}{\mathrm{d}\nu} + \frac{C_\chi}{30h^2c^2}\frac{\mathrm{d}^2[\epsilon(\nu)/\nu]}{\mathrm{d}\nu^2}\right\} \quad (1)$$

where $\vec{F}$ is the applied electric field, f is the local field correction factor, c is the speed of light, and h is Planck's constant. χ is the angle between the applied electric field and the polarization vector of the probe light. The use of derivatives of the absorption spectrum stems from the assumption that changes in the line shape because of the applied electric field are small as compared to the width of the spectral line. This assumption allows the line shape function (usually Lorentzian or Gaussian) to be expanded in a Taylor series about the zero field band. The 0th, 1st, and 2nd terms in this expansion yield the 0th, 1st, and 2nd derivatives of the absorption spectrum. The changes in dipole moment and polarizability are then obtained from the coefficients of the 1st and 2nd derivatives, respectively, used to fit the Stark spectra. In addition, the use of polarized light to obtain the spectrum can provide the angle between these electronic structure properties and the transition dipole moment being probed. From the above description, it is clear that there is the intrinsic requirement for a high quality low-temperature absorption spectrum to properly fit the Stark spectrum.

Even for high quality spectra, the numerical differentiation of the raw absorption spectrum often leads to noisy derivative spectra. It is therefore customary to first fit the absorption spectrum using a series of Gaussian functions. While it is tempting to see this as a spectral deconvolution, the importance of this procedure is to smooth the spectrum to produce derivatives that can be used in the analysis of the Stark spectrum. For example, the room-temperature absorption spectrum of OYE can be fitted to a set of Gaussians reasonably well, where each vibronic feature is assigned to one Gaussian function (fit not shown). However, when this is done the Gaussians have a wide range of widths, even within a single electronic transition. A more useful fit for the analysis of the Stark spectrum is obtained by using (at least) two Gaussians for each vibronic feature in Band I, and one Gaussian for each feature in Band II. Despite this, no claim is made that the Gaussian fit is unique, and in fact the fitting program treats the Gaussian parameters (width, center, and amplitude) as initial parameters that are adjusted as needed to fit both the Stark and the absorption spectra simultaneously.

Fitting the Spectra. Multiple Stark spectra were obtained for each molecule at different χ values and external field values. These data were paired with low-temperature absorption spectra and fitted to obtain the A_χ, B_χ, and C_χ coefficients (see eq 1) as described in a previous publication (*19*). Error bars for the fitted parameters presented below were obtained by a sensitivity analysis where the mean A_χ, B_χ, and C_χ coefficients were used as inputs to generate simulated input A_χ, B_χ, and C_χ parameter sets with a varying degree of random error (*21*). The error was adjusted to encompass the experimental error of all of the fitted A_χ, B_χ, and C_χ coefficients. The Stark spectra were fitted using several different absorption spectra. The derived values resulting from the different fits were averaged together to reduce the bias resulting from the use of a single absorption spectrum or Gaussian fit to that spectrum. The programming for the absorption and Stark spectra fitting were performed using MATLAB (The Mathworks, Inc.).

Instrumentation. The Stark spectrometer has been described in detail previously (*19*, *22*). Briefly, A 150W Xe arc lamp was filtered through a 1/8 m monochromator. This light was polarized by a Glan−Taylor calcite polarizer and passed through the optical cuvette in the dewar. The cuvette was connected to an AC high voltage amplifier driven by the sine-wave generator of a lock-in amplifier at about ω ~200 Hz. Voltages of above 4000 V peak-to-peak (about 6.3×10^5 volts/cm) could be applied without breakdown of the sample. The transmitted light was focused onto a UV-enhanced silicon photodiode using a short focus quartz lens. The photocurrent was amplified in a current-to-voltage amplifier (Keithley 427) and detected by the digital lock-in

amplifier at 2ω (SRS 830). The amplified photocurrent was also digitized to 16-bit accuracy using the A/D port in the lock-in amplifier.

The band-pass of the monochromator was set to 2 nm, but the monochromator was stepped in equal-energy increments (e.g., $\Delta E = 120$ cm^{-1}). While this may seem to distort the spectrum, the opposite is true. We use this procedure since equal-wavelength stepping tends to undersample the blue side and oversample the red side of the spectrum. For example, a 2 nm band-pass at 300 nm will result in an energy increment of $\Delta E = 221$ cm^{-1}, while the same increment at 700 nm results in $\Delta E = 41$ cm^{-1}. Since the line shape is a property of the energy and not the wavelength, equal-energy stepping will reproduce the line shape more accurately. Using $\Delta E = 120$ cm^{-1} stepping, a single increment from 300 nm (33 333 cm^{-1}) will put the monochromator at 301.1 nm (33 123 cm^{-1}) so that $\Delta\lambda = 1.1$ nm. At 700 nm (14 286 cm^{-1}), the increment will be 705.9 nm (14 166 cm^{-1}) or $\Delta\lambda = 5.9$ nm.

An optically transparent electrically conductive capacitor was constructed from two aluminosilicate slides that were coated on facing sides with a transparent conductive layer of indium tin oxide ($R = 100$ Ω/cm, Delta Technologies Ltd.). The two slides were separated by a thin Kapton film (C. S. Hyde, 18-1F), which set the path length at 32 μm (± 3 μm) as determined by measuring interference fringes at room temperature. This optical capacitor was mounted on a Teflon rod. The rod holding the cuvette was attached to a rotation stage so that the angle of the cuvette ($\pm 1°$) could be changed relative to the direction of the polarization vector of the probe light. Electrical connection was made to the sample using alligator clips with a piece of indium foil to ensure good contact at cryogenic temperatures. The cuvette was plunged into an optical dewar containing liquid nitrogen, and an excellent optical glass was formed. Helium gas was passed over the surface of the liquid nitrogen to discourage bubbling and Schlieren effects.

RESULTS

Low-Temperature Absorption Spectra: OYE. Very few low temperature (77 K) absorption spectra of flavoproteins have been reported, and to our knowledge no 77 K spectra have been measured for OYE. The absorption spectrum of oxidized flavin in the UV−vis region is characterized by two relatively strong $\pi \rightarrow \pi^*$ transitions centered around 450 and 370 nm and are hereafter referred to as Band I and Band II, respectively. At room temperature in aqueous buffer the spectrum is relatively featureless, although it is clear that both Bands I and II have some underlying vibronic structure that is amplified in nonpolar solvents and/or at low temperature. The resolution of this progression in flavoproteins is often taken to indicate that the isoalloxazine is tightly bound in the cofactor binding site, which itself is usually relatively nonpolar.

The room temperature (RT) and 77 K (LT) absorption spectra for OYE are shown in Figure 1a. From the figure, the maximum extinction of the RT spectrum is $\epsilon_{max}^{464} = 12\,883$ M^{-1} cm^{-1}, which is in reasonable agreement (about 10% higher) with the literature value (*20*). The use of derivatives has been shown to provide a more accurate determination of the peak center (*23*), and the 2nd derivatives

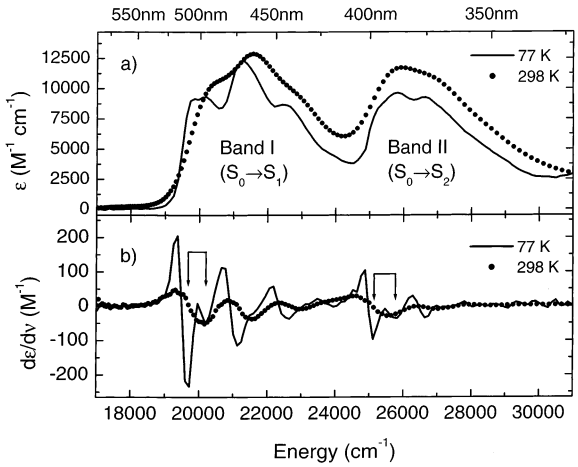

FIGURE 1: (a) 77 K (− − −) and 298 K (•••) spectra of oxidized OYE are given at 368 μM in phosphate buffer, pH 7.0. Vibronic structure evident at room temperature becomes more highly resolved at low temperature. (b) The 2nd derivative of the absorption spectra. The minima in the derivative spectra correspond to peaks in the absorption spectra. Doublets can be seen in both Bands I and II at low temperature using this technique. The first doublets for bands I and II are indicated by sets of braced arrows.

Table 1: OYE Absorption Spectra

RT abs. spectrum 2nd deriv. (cm^{-1})	LT abs. spectrum 2nd deriv. (cm^{-1})	$\Delta\nu$
	Band I	
20 161	19 715	469
	20 184	
21 552	21 122	469
	21 591	
22 936	22 647	586
	23 233	
24 272	23 936	352
	24 288	
(1370 ± 24)	(1388 ± 185)	(469 ± 83)
	Band II	
25 510	25 109	703
	25 812	
27 027	26 633	704
	27 337	
28 736	28 040	469
	28 509	
(1613 ± 96)	(1407 ± 144)	(625 ± 111)

of the raw RT and LT spectra are shown in Figure 1b. The apparent vibronic progression in Band I is composed of three peaks with a spacing of 1370 ± 24 cm^{-1}. Band II is composed of two peaks with a spacing of 1613 ± 96 cm^{-1}. These were determined by taking differences for the peak positions for the RT 2nd derivative spectra cited in Table 1.

The LT spectrum is red-shifted relative to the RT spectrum and is more highly structured, as would be expected. The LT maximum, $\epsilon_{max}^{470} = 12\,379$ M^{-1} cm^{-1} is red-shifted by about 430 cm^{-1} (~ 6 nm). The 2nd derivative spectra show clearly that each vibronic feature in the LT spectrum is composed of two nearly overlapping lines that we refer to as a doublet. The peak assignments are found in Table 1. The splitting between these doublets is 469 ± 83 and 625 ± 111 cm^{-1} for Bands I and II, respectively. To our knowledge, this is the first observation of this behavior and is indicative of protein−cofactor interactions (see Discussion). These new features make a comparison with the RT spectrum more difficult, but it appears that the most intense

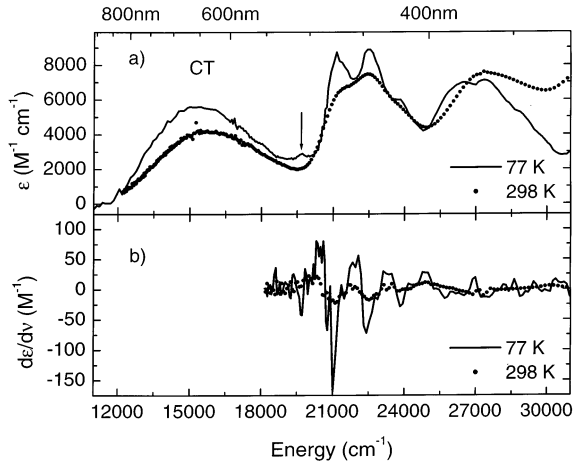

FIGURE 2: (a) 77 K (− − −) and 298 K (•••) spectra of oxidized OYE in the presence of 0.5 mM *p*-chlorophenol in phosphate buffer, pH 7.0. A strong broad band centered at about 16 000 cm^{-1} has been ascribed to a charge-transfer transition. The small but reproducible feature at 507 nm is indicated by the arrow. (b) 2nd derivative spectra of the absorption spectra. The derivatives become noisy below 18 000 cm^{-1} so that this spectral region has been truncated.

Table 2: OYE:*p*-Cl Phenol Complex Absorption Spectra

RT abs. spectrum 2nd deriv. (cm^{-1})	LT abs. spectrum 2nd deriv. (cm^{-1})
CT Band	
15 576	15 333
Band I	
	19 715
21 097	21 005
22 523	22 412
23 697	23 819
	25 695
(1300 ± 126)	(1495 ± 225)
Band II	
26 882	26 516
27 322	27 219
	28 860

peak of the doublet is shifted by 469 ± 83 cm^{-1} to lower energy in Band I, while the weaker peak is unshifted as compared to the unresolved RT vibronic band.

The vibronic band spacing for the LT spectrum are 1388 ± 185 and 1407 ± 144 cm^{-1} for Bands I and II, respectively. In this case, the vibronic spacing was obtained by averaging the energy difference for the lower energy pairs and the upper energy pairs of the doublet. The RT and LT progression intervals agree within the stated accuracy. It should be noted that the RT spectrum was recovered on warming the LT samples, suggesting that cold denaturation is not responsible for the doublet splitting or spectral shifts.

Low-Temperature Absorption Spectra: OYE:p-Cl Phenol Complex. The room-temperature and low-temperature absorption spectrum of the CT complex are shown in Figure 2a. In the LT spectrum, only the CT transition is slightly red-shifted relative to the RT spectrum. The maximum extinction coefficient for the CT band at room temperature is about 4200 M^{-1} cm^{-1} at 642 nm. This compares well with the literature value of 4400 M^{-1} cm^{-1} at 645 nm (*20*). The maximum extinction coefficient for the low-temperature CT band is about 6000 M^{-1} cm^{-1} at 652 nm, an increase of about 43%. Comparison with the OYE spectra shows that the line

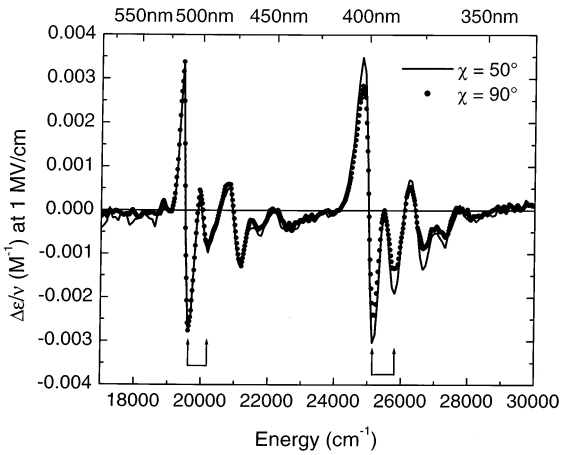

FIGURE 3: Stark spectra of oxidized OYE at low temperature. The traces consist of averages of at least three data sets per polarization (50 and 90°). The data have been normalized to 1 MV/cm for comparison. The first doublets for Bands I and II are indicated by sets of braced arrows.

widths of the complex spectrum are greater than for OYE alone. In addition, there is a reproducible feature at 507 nm (19 715 cm^{-1}) that is absent in the room temperature spectrum and to our knowledge has not been previously observed.

The spacings of the vibronic components are 1300 ± 126 and 1495 ± 225 cm^{-1} for the RT and LT progressions in Band I, respectively (see Table 2). The data are too noisy to retrieve convincing spacings for Band II. Figure 2b shows the second derivative of the absorption spectra. These have been truncated at about 18 000 cm^{-1} because the derivative spectra become too noisy below this limit. Some evidence for doublet structure is seen, but the features are not well-resolved. No vibronic structure is seen for the CT band. Although there is clear spectral narrowing for the $\pi \rightarrow \pi^*$ bands at low temperature, the CT band is still very broad.

Stark Spectroscopy: OYE. Low-temperature Stark spectra for OYE in a glycerol/buffer glass are shown in Figure 3. The spectra are the average of more than three data sets for each angle and were obtained with an applied field of about $4.4-5.8 \times 10^5$ V/cm. The two traces show the effect of the applied electric field on the absorption spectrum when the polarization of the probe beam is 90 or 50° to the direction of the applied field. The averaged spectra have been normalized to 10^6 V/cm for comparison.

The Stark spectra were analyzed to obtain changes in the electronic distribution of the FMN cofactor in going from the ground to excited singlet states. The fitting required only two sets of A_χ, B_χ, and C_χ coefficients; one set per band. A sample fit to a typical single data set at an applied field of 5.2×10^5 V/cm and $\chi = 50°$ is shown in Figure 4. The Band I fit is indicated by the open circles, and the Band II fit is indicated by the open triangles. It can be seen that the fitting procedure isolates the coefficients for Bands I and II quite well. If this were not the case, then there would be more overlap between the fits in the 24 000 cm^{-1} region. It is worth pointing out that the doublets, which are very well-separated in the Stark spectra, do not require any additional fitting coefficients and therefore have the same initial and final electronic states within the particular electronic transition. This suggests that the doublet structure is not due to

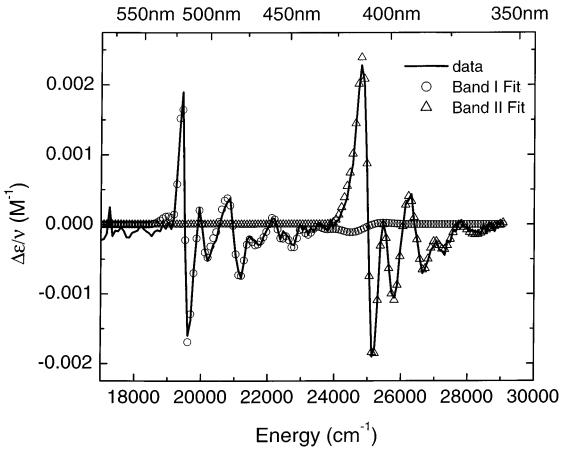

FIGURE 4: Sample OYE data set normalized to 10^6 V/cm (—) and the fit to the data for Band I (○) and Band II (△).

Table 3: OYE Electronic Structure Parameters[a]

	$tr\Delta\alpha$ (Å^3·f^2)	m·$\Delta\alpha$·m (Å^3·f^2)	$\lvert\Delta\mu\rvert$ (D·f)	ζ_A (deg)
Band I	51 ± 5	23 ± 2	2.9 ± 0.3	57 ± 1
	(22 ± 5)	(32 ± 15)	(2.5 ± 0.2)	(58 ± 11)
Band II	198 ± 40	161 ± 32	7.1 ± 0.7	40 ± 4
	(162 ± 34)	(183 ± 100)	(7.8 ± 0.5)	(30 ± 9)

[a] Parentheses indicates values for N(3)-methylated flavin in 2-MTHF.

changes in the electronic structure of the FMN cofactor upon freezing.

The fitted electronic structure parameters are very close to those measured for flavins in organic glasses and are given in Table 3. A comparison with N(3)-methyl-N(10)-isobutyl-7,8-dimethylisoalloxazine in 2-methyltetrahydrofuran (*19*) (in parentheses below the protein values) shows essentially no change in the electronic properties of the flavin because of the protein environment as measured by Stark spectroscopy. This is in spite of the fact that OYE lowers the midpoint potential of the FMN oxidized → semiquinone anion couple by about 15 mV relative to free FMN (*3*). The Stark spectroscopic result is not surprising, however, as it reports on differences in the ground and excited electronic properties of the FMN cofactor and not on their absolute values. Though there is good agreement between protein and the simple solvent parameters in this system, we have observed significant differences in these parameters for other flavoproteins (data not shown). These observations will be the focus of a future communication.

Stark Spectroscopy: OYE:p-Cl Phenol Complex. The Stark spectra of the charge-transfer complex at two different angles are shown in Figure 5. The most significant difference between the complex and the uncomplexed OYE spectra is the appearance of a large 2nd derivative feature at about 15 000 cm^{-1} (~667 nm). This band appears to overlap Band I until about 22 500 cm^{-1} (~444 nm). Furthermore, the Stark spectrum of the CT band is not simply a single 2nd derivative but consists of four bands at 12 710, 14 491, 15 815, and 17 280 cm^{-1}, giving a spacing of 1523 ± 191 cm^{-1} (indicated by the braced arrows). The band positions were determined from a fit of the CT/Band I system as described below. This spacing is the same as that obtained for the LT absorption spectrum of the OYE CT complex Band I (see Table 2). We come back to this observation in the Discussion.

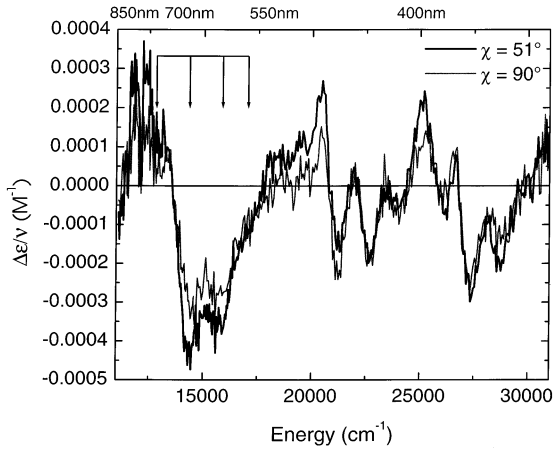

FIGURE 5: Stark spectra of the OYE:*p*-Cl phenol complex at low temperature. The data have been normalized to 1 MV/cm for comparison. The largest feature is the structured band around 15 000 cm^{-1}. The braced arrows indicate the vibronic structure. The structure in this region is reproducible from scan to scan.

Table 4: OYE:*p*-Cl Phenol Electronic Structure Parameters[a]

	$tr\Delta\alpha$ (Å^3·f^2)	m·$\Delta\alpha$·m (Å^3·f^2)	$\lvert\Delta\mu\rvert$ (D·f)	ζ_A (deg)
CT band	376 ± 75	210 ± 42	12 ± 1	0 ± 10
Band I	68 ± 10	26 ± 4	2.8 ± 0.6	42 ± 8
	[102 ± 31]	[29 ± 9]	[2.7 ± 0.5]	[34 ± 7]
Band II	[376 ± 75]	[229 ± 46]	[8.2 ± 1.6]	[13 ± 3]

[a] Brackets indicate that the parameters were fitted to spectra truncated to include only Bands I and II (21 500 cm^{-1} < ν < 31 000 cm^{-1}).

Overall, the CT spectrum is noisier than that for OYE alone. This is due to the much broader absorption spectrum of the complex as compared to the OYE alone. Using the zero-crossing points of the lowest energy vibronic band of Band I as a gauge of the line width, the bands of the OYE:*p*-Cl phenol complex spectra are about 3× larger than the OYE vibronic bands. This difference leads to a factor of about 9 for the ratio of the magnitude of the OYE spectrum as compared to that of the complex, purely because the 2nd derivative amplitude depends inversely on the square of the line width. With this in mind, we should expect that the CT band will have a much larger dipole moment change than either Band I or II, as its Stark spectrum is greater in intensity than the $\pi \rightarrow \pi^*$ transitions but inherently much broader. It is also worth noting that the difference between 90 and 51° traces is much greater for the CT band than for Band II, indicating that the angle between the CT transition dipole moment and $\Delta\mu_{CT}$, ζ_A^{CT}, is smaller than for Band II.

Because of the problem of overlapping transitions, Stark coefficients for the complex spectra were obtained in two stages. First, the coefficients for Bands I and II were obtained by fitting only over the region from 23 000−31 000 cm^{-1} to remove a potential bias of the Band I values toward the 15 000 cm^{-1} feature (Band I/Band II fit). Then the CT and Band I values were obtained by fitting the spectra from ~11 000−25 000 cm^{-1} (CT/Band I fit). This procedure provides a check on the accuracy of the fit for all three bands since both fits must provide Band I values that are in agreement. All of these values are given in Table 4.

The agreement between Band I values for OYE and the OYE:*p*-Cl phenol complex is excellent, whether these parameters were obtained from the CT/Band I or Band I/Band II fit. Only the ζ_A value is different: ~38° for the

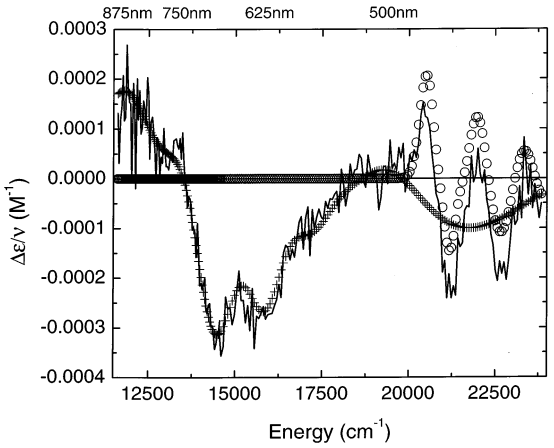

FIGURE 6: Sample fit to the spectral region containing the CT band (+) and Band I (○). See text for details.

complex versus 57° for OYE. It is possible that this is an artifact of the fitting procedure, but the value appears relatively stable between the two fitting regimes. We take this difference as significant, indicating that either the S_0 (ground) state and/or the S_1 state are mixed with the CT state. Further justification for this conclusion is found in the ζ_A value for the CT band itself (see below). The parameters for Band II are in good agreement with those for OYE alone, although there is no reason for them to agree perfectly.

The electronic structure parameters for the CT band are dramatically different from either Band I or Band II. $\Delta\mu_{CT}$ is about 12 D·*f*, as compared to 2.8 D·*f* for Band I and 8.2 D·*f* for Band II. Since these values presumably share the same local field correction factor (*f*), this represents a significant charge shift for the 664 nm band and essentially confirms its CT character. For a dielectric constant of 5 ($f = 1.36$ for a spherical dielectric cavity), $\Delta\mu_{CT} = 8.8$ D, giving a single electron shift of about 1.8 Å from the phenolate donor to the FMN acceptor. The crystal structure of OYE complexed with *p*-hydroxybenzaldehyde gives a ligand−FMN distance of about 3.6 Å (*14*). Our results suggest that the electron is equidistant between the ligand and the cofactor. $\zeta_A^{CT} = 0 \pm 10°$ agrees with what is expected for the angle between $\Delta\mu_{CT}$ and the transition dipole moment direction for a true charge-transfer band, which is thought to lie along the direction of charge transfer (*24*).

The $tr\Delta\vec{\vec{\alpha}}$ value of 376 Å^3·f^2 for the CT band is significantly larger than that for Band I (~75 Å^3·f^2) but about the same as that for Band II. However, the difference polarizability for Band II is larger than that for Band I in both OYE alone and in flavins in simple solvents. In the case of the CT band, a higher polarizability change is expected if the electron undergoes more facile transfer from donor to acceptor. This value is large as compared to aromatic molecules such as coumarin (*25*) but more in the range of polyenes, where significant charge delocalization is observed (*26*−*28*). In this respect, the mean polarizability change may show a linear correlation with $h\nu_{CT}$ since polarizability should be related to the ionization potential and correlate with the Hammett para parameter, σ. A benefit in using Stark spectroscopy may be that the $tr\Delta\vec{\vec{\alpha}}$ (and $\vec{m}\cdot\Delta\vec{\vec{\alpha}}\cdot\vec{m}$, the projection of the difference polarizability along the transition dipole moment) can provide a measure of the polarizability of the flavin at the molecular level.

A sample fit of the CT and Band I parameters to a representative data set truncated before Band II is shown in Figure 6. The fit to the CT band is represented by (+) and Band I by (o). Several comments are in order. First, the expanded scale and fit both highlight the double minimum around 15 000 cm^{-1}. The significance of this is left to the Discussion. Second, the component of the CT fit at about 22 000 cm^{-1} may represent a scattering artifact in the low-temperature absorption spectrum since there is no provision to remove scattering from the fitting procedure for the absorption spectra. While this is a concern, not all data sets led to this overlap of CT and Band I fits. It does point out that the quality of the low-temperature absorption spectrum is critical where there are overlapping transitions. However, we feel that the error bars for the fitted parameters are reasonable.

DISCUSSION

The observation of doublet splitting in the vibronic progressions for Bands I and II is not confined to OYE. We have observed similar splittings (data not shown) to a greater or lesser degree in other flavoproteins at low temperature, including glutathione reductase (FAD), lipoamide dehydrogenase (FAD), DNA photolyase (FAD), and flavodoxin (FMN). The latter two flavoproteins are monomeric in flavin, while the others are dimeric. This suggests that the doublet structure is not unique to OYE or due to cold denaturation. It is difficult at this time to rationalize the degree of splitting from protein to protein, but the doublet structure is visible irrespective of whether FMN or FAD is the cofactor. However, we have observed a similar doublet structure in the low-temperature Stark spectra of flavins in a glycerol/H_2O glass (*22*) but not in other simple solvents such as ethanol, *n*-butanol, or 2-methyltetrahydrofuran (*19*). This result suggests that hydrogen bonding is perturbing the structure of the isoalloxazine ring sufficiently to split the accidental degeneracy of the overlapping vibronic progressions so that the doublet structure emerges. Dutta et al. have observed similar shifts in the CARS spectra of FMN and FAD and attributed this shift to hydrogen bonding at N(3)−H (*29*). Our results rule this out as an explanation for the absorption/Stark spectral shifts since the splitting is observed for a N(3)-methylated flavin in a glycerol/H_2O glass (*22*).

Strong hydrogen bonding at the C(2) and C(4) carbonyl groups has been identified in OYE (*30*). In this case, the doublet would consist of a vibration that is insensitive to the carbonyls but isoenergetic with a vibrational mode that would be sensitive to hydrogen bonding and/or deuterium isotope effects. Lively and McFarland have performed a normal-mode analysis of lumiflavin to address the issue of hydrogen bonding-induced shifts in vibrations involving these carbonyl groups (*31*). However, the shifts they calculate are an order of magnitude too small to explain our observations, except for the effect of hydrogen bonding on N(3)−H, where the shift is about 100 cm^{-1}. Again, our N(3)-methylated flavin result rules out this possibility. With our present data, we cannot rule out protein-induced flavin deformation as an important factor since the splitting differs from protein to protein. Low-temperature absorption spectroscopy using D_2O could reveal much information on these flavin−protein interactions. In general, low-temperature absorption spectroscopy of flavoproteins is underutilized.

Another important result from these experiments is the confirmation of the charge-transfer band in the OYE:*p*-Cl phenol complex. This points the way to an examination of CT interactions in virtually any flavoprotein that has an optically accessible CT transition. In addition, the difference between spectra taken with different probe polarizations suggests that the angle of charge displacement can be obtained from an analysis of these data and that they agree well with the results for the transition moment direction of the CT band of a lumiflavin-2-aminobenzoic acid complex (*24*), which to our knowledge is the only such measurement of the CT transition dipole moment direction involving flavins. Finally, an analysis of the changes in the electronic distribution of the S_1 and S_2 states because of the protein matrix (relative to flavin in simple solvent) can be achieved, even in the presence of CT complexation.

By way of comparison, Palfey has performed ZINDO calculations based on the OYE-*p*-hydroxybenzaldehyde structure (*14*) consisting of the ligand; FMN cofactor; and the residues Pro34, Pro35, Leu36, Thr37, Gln114, Glu189, His191, Asn194, Arg243, and Tyr375 (B. Palfey, University of Michigan, Ann Arbor, personal communication). These calculations were performed using a dielectric continuum solvation model for a dielectric constant of $\epsilon = 9$ and a cavity radius of 8.4 Å. A CT band is obtained at 712 nm with a $\Delta\mu_{CT}^{ZINDO} = 11.8$ D. This is about 40% larger than our result with $f = 1.36$. A better match is obtained if the local field correction factor is set to $f = 1.2$, giving $\Delta\mu_{CT} = 10$ D, but this requires that $\epsilon = 2$. The calculated band center is about 950 cm^{-1} too low, while the band center for the Bands I and II are blue-shifted by 740 and 1630 cm^{-1}, respectively. The difference dipole moments for these transitions are $\Delta\mu_{I}^{ZINDO} = 0.72$ D and $\Delta\mu_{II}^{ZINDO} = 5.4$ D. These can be compared to our experimental values of $\Delta\mu_{I} = 2.1$ D and $\Delta\mu_{II} = 6.0$ D for $f = 1.36$.

The structure observed in the Stark spectrum for the CT transition was unexpected but may be highly significant. The band separation of ~1500 cm^{-1} observed in the Stark spectrum of the CT band is the same spacing obtained for the vibronic bands of the FMN cofactor in OYE and in Band I/II of the complex. However, no structure was observed in the Tyr 98 → Trp CT mutant in *Desulfovibrio vulgaris* oxidized flavodoxin (*11*) (results not shown) within the signal-to-noise. This suggests that the bands arise from a particular interaction between the phenolate and the FMN molecules. Vibrational progressions in CT bands have been observed previously for crystals of the anthracene-trinitrobenzene complex (*32*). The source of the 1400 cm^{-1} progression was thought to be the anthracene donor. Earlier observations of vibrational structure in the CT spectra of hydrocarbon/tetrahalo *p*-benzoquinones in chloroform arrived at the conclusion that the ~200 cm^{-1} progression was due to the acceptor.

More recently, Zheng et al. have used resonance Raman spectroscopy to explore the OYE−phenolate system with high resolution. Excitation into the CT band led to large amplification of the flavin and ligand bands coupled to the charge-transfer transition. Several of the enhanced phenolate bands would be candidates for the 1500 cm^{-1} progression observed in the Stark spectrum and consist of in-plane C−H stretching. In other work, they found enhancement of flavin modes involving the N(5)−C(4a)−C(10a)−N(1) region where electron donation is thought to occur (*33*). It is unclear at this point as to whether the progression we have observed in the Stark spectrum is due to the donor or acceptor, but it should be possible to sort this out using different *p*-halophenolate ligands (e.g., *p*-bromophenol).

In summary, we have obtained the first Stark spectrum of a flavoprotein, OYE, and its CT complex with *p*-chlorophenol. For OYE, the fitted parameters agree well with those for flavins in simple solvents, indicating that the protein matrix does not greatly modulate the electronic structure of the flavin cofactor. The parameters found for the *p*-Cl phenolate complex show a large charge displacement consistent with transfer of an electron from the electron-rich phenolate donor midway to the electron-deficient FMN acceptor. Structure in the Stark CT spectrum points out the crystalline nature of the CT complex, at least for this system. Finally, the ability to quantitatively measure the degree and direction of charge transfer in flavoproteins and protein−ligand complexes will allow us to more rigorously assess the role of charge transfer in flavoprotein catalysis.

ACKNOWLEDGMENT

This paper is dedicated to the memory of Prof. Vincent Massey. Prof. Massey also provided the OYE used in these experiments. We wish to thank Dr. Bruce Palfey of the University of Michigan, Ann Arbor for supplying the ZINDO results for the OYE complex and for a critical reading of the manuscript. We would also like to thank Prof. Richard Swenson for flavodoxin and flavodoxin mutant protein samples and Profs. Steve Boxer (Stanford), Stefan Franzen (NC State), and Linda Peteanu (CMU) for useful discussions.

REFERENCES

1. Slifkin, M. A. (1971) *Charge-Transfer Interactions of Biomolecules*, Academic Press, London.
2. Massey, V., and Ghisla, S. (1974) *Ann. N.Y. Acad. Sci. 227*, 446−65.
3. Stewart, R. C., and Massey, V. (1985) *J. Biol. Chem. 260*, 13639−47.
4. Hopkins, N., and Williams, C. H., Jr. (1995) *Biochemistry 34*, 11757−65.
5. Williams, C. H., Jr. (1992) *Chem. Biochem. Flavoenzymes 3*, 121−211.
6. McCormick, D. B. (1977) *Photochem. Photobio. 26*, 169−182.
7. Zheng, Y., Massey, V., Schaller, A., Palfey, B. A., and Carey, P. R. (2001) *J. Raman Spec. 32*, 579−86.
8. MacFarlane, A. W., IV, and Stanley, R. J. (2001) *Biochemistry 40*, 15203−14.
9. Mulliken, R. S., and Person, W. B. (1969) *Molecular Complexes*, Wiley-Interscience, New York.
10. Foster, R. (1969) *Organic Charge-Transfer Complexes*, Academic Press, London.
11. Swenson, R. P., and Krey, G. D. (1994) *Biochemistry 33*, 8505−14.
12. Xu, D., Kohli, R. M., and Massey, V. (1999) *Proc. Natl. Acad. Sci. U.S.A. 96*, 3556−61.
13. Abramovitz, A. S., and Massey, V. (1976) *J. Biol. Chem. 251*, 5327−36.
14. Fox, K. M., and Karplus, P. A. (1994) *Nature Structure (London) 2*, 1089−105.
15. Stanley, R. J. (2001) *Antioxid. Redox Signaling 3*, 847−66.
16. Bublitz, G. U., and Boxer, S. G. (1997) *Annu. Rev. Phys. Chem. 48*, 213−42.
17. Chowdhury, A., Peteanu, L. A., Webb, M. A., and Loppnow, G. R. (2001) *J. Phys. Chem. B 105*, 527−34.
18. Liptay, W. (1974) in *Excited States* (Lim, E. C., Ed.) pp 129−229, Academic Press, Inc., New York.
19. Stanley, R. J., and Siddiqui, M. S. (2001) *J. Phys. Chem. A 105*, 11001−8.

20. Brown, B. J., Deng, Z., Karplus, P. A., and Massey, V. (1998) *J. Biol. Chem. 273*, 32753−62.
21. Press, W. H., Flannery, B. P., Teukolsky, S. A., and Vetterling, W. T. (1988) *Numerical Recipes in C The Art of Scientific Computing*, Cambridge University Press, New York.
22. Stanley, R. J., and Jang, H. (1999) *J. Phys. Chem. A 103*, 8976−84.
23. Massey, V., Schopfer, L. M., and Dunham, W. R. (1984) in *Flavins Flavoproteins, Proc. Int. Symp., 8th* pp 191−210.
24. Shieh, H.-S., Ghisla, S., Hanson, L. K., Ludwig, M. L., and Nordman, C. E. (1981) *Biochemistry 20*, 4766−74.
25. Chowdhury, A., Locknar, S. A., Premvardhan, L. L., and Peteanu, L. A. (1999) *J. Phys. Chem. A 103*, 9614−25.
26. Locknar, S. A., and Peteanu, L. A. (1998) *J. Phys. Chem. B 102*, 4240−6.
27. Mathies, R., and Stryer, L. (1976) *Proc. Natl. Acad. Sci. U.S.A. 73*, 2169−73.
28. Liptay, W., Walz, G., Baumann, W., Schlosser, H. J., Deckers, H., and Detzer, N. (1971) *Z. Naturforsch. A 26*, 2020−38.
29. Dutta, P. K., Nestor, J. R., and Spiro, T. G. (1977) *Proc. Natl. Acad. Sci. U.S.A. 74*, 4146−9.
30. Fox, K. M., and Karplus, P. A. (1999) *J. Biol. Chem. 274*, 9357−62.
31. Lively, C. R., and McFarland, J. T. (1990) *J. Phys. Chem. 94*, 3980−94.
32. Eckhardt, C. J., and Eckhardt, H. (1980) *J. Am. Chem. Soc. 102*, 2887−92.
33. Zheng, Y., Wagner, M. A., Jorns, M. S., and Carey, P. R. (2001) *J. Raman Spec. 32*, 79−92.

BI0268908